Quantitative MRI in obesity & reno-cardiovascular function

Dekkers, I.A.

5

^{1}H-MRS for the assessment of renal triglyceride content in humans at 3T: a primer and reproducibility study

IA Dekkers, P de Heer, MB Bizino, APJ de Vries, HJ Lamb.

J Magn Reson Imaging. 2018 Aug;48(2):507-513.

ABSTRACT

Background

Renal steatosis (fatty kidney) is a potential biomarker for obesity-related renal disease, however non-invasive assessment of renal fat content remains a technical challenge.

Objectives

To evaluate reproducibility and explore clinical application of renal metabolic imaging for the quantification of renal triglyceride content (TG) using proton magnetic resonance spectroscopy (^{1}H-MRS).

Methods

Twenty-three healthy volunteers (mean age 30.1 ± 13.4 years), and 15 patients with type 2 diabetes mellitus (T2DM) (mean age 59.3 ± 7.0 years) underwent ^{1}H-MRS using the Single-voxel Point Resolved Spectroscopy (PRESS) sequence at a clinical MRI scanner. Intra- and inter-examination reproducibility of renal TG was assessed in healthy volunteers, and compared to T2DM patients. Intra-examination differences were obtained by repeating the ^{1}H-MRS measurement directly after the first ^{1}H-MRS without repositioning of the subject or changing surface coil and measurement volumes. Inter-examination variability was studied by repeating the scan protocol after removal and replacement of the subject in the magnet, and subsequent repositioning of body coil and measurement volumes. Reproducibility was determined using Pearson's correlation and Bland-Altman-analyses. Differences in TG% between healthy volunteers and T2DM patients were assessed using the Mann-Whitney U test.

Results

After logarithmic (log) transformation both intra-examination (r=0.91, n=19) and inter-examination (r=0.73, n=9) measurements of renal TG content were highly correlated with first renal TG measurements. Intra-examination and inter-examination limits of agreement of renal log TG% were respectively [-1.36%, +0.84%] and [-0.77%, +0.62%]. Back-transformed limits of agreement were [-0.89%,+0.57%] and [-0.55%, +0.43%] multiplied by mean TG for intra- and inter-examination measurements. Overall median renal TG content was 0.12% [0.08, 0.22; 25th percentile, 75th percentile] in healthy volunteers and 0.20% [0.13, 0.22] in T2DM patients (P=0.08).

Conclusion

Renal metabolic imaging using 3T ^{1}H-MRS is a reproducible technique for the assessment of renal triglyceride content.

INTRODUCTION

The strong increase in the prevalence of obesity has coincided with an increase in chronic kidney disease (1). Lipid nephrotoxicity due to the accumulation of lipids in tubular or glomerular cells of the kidney, also known as renal steatosis or 'fatty kidney' (2), has been proposed as an important pathophysiological pathway of obesity-related renal disease (3). Furthermore, renal steatosis has been linked to renal hyperfiltration (4) and type 2 diabetic nephropathy (5). Studies evaluating possible biological mechanisms have remained confined to animal models (6–8), as it is unethical to perform kidney biopsies without clear evidence of (advanced) renal disease, indicating the need for non-invasive biomarkers of fatty kidney.

The ability of proton magnetic resonance spectroscopy (^{1}H-MRS) to non-invasively quantify triglycerides based on tissue specific metabolite spectra makes this technique a unique imaging modality to study obesity-related renal disease. ^{1}H-MRS has evolved over past years as a valid non-invasive technique to study lipid content in tissue such as liver (9), muscle (10), and heart (11). Technical advances of spectroscopy have created the opportunity to also explore metabolic and physiologic processes in the kidney. Renal triglyceride (TG) content measured using ^{1}H-MRS has previously been described at 1.5T (12) and was recently validated against gold-standard enzymatic assay in ex-vivo porcine kidneys (similar sized to human kidneys) (13).

As higher field strengths result in a better resolution and spectral peak quantification, we aimed to improve the ^{1}H-MRS protocol for renal TG measurements at 3T. We examined intra- and inter-examination reproducibility and explored the application of renal metabolic imaging in type 2 diabetes patients.

MATERIAL AND METHODS

Participants

The Institutional Review Board of our institution approved the study protocol and study design. Written informed consent was obtained from all participants in the present study.

This study consisted of healthy volunteers who participated in the reproducibility analyses, and type 2 diabetes (T2DM) patients. The healthy volunteers were recruited via a local database of people who participate regularly in technical MRI development studies (≥18 years and without known renal disease). The type 2 diabetes patients were the first 15 consecutive patients who were recruited via the endocrinology outpatient clinic to undergo renal metabolic imaging. Inclusion criteria were: age between 18 to 70 years, overweight or obesity (Body mass index, BMI >25 kg/m^{2}), type 2 diabetes with HbA1c levels between 7 to 10%, moderately impaired to normal renal function (estimated glo-

merular filtration rate >60 ml/min/1.73m²), and normal blood pressure (<150/85 mmHg). All renal TG content and serum measurements were performed after overnight fasting, or at least 4 hours fasting to exclude potential dietary effects.

Data acquisition

MR examinations were performed on a 3T Ingenia whole-body MRI scanner (Philips Healthcare, Best, The Netherlands). Spectra were obtained from the parenchyma of the left kidney. The standard posterior (12 channels) and anterior (16 channels) torso/cardiac surface receiver coils were used with the participants placed in supine position. After a standard survey, breath-hold Dixon water/fat scans were acquired of the kidney in three directions at end-expiration. Planning of the single ^{1}H-MRS voxel (40 x 10 x 10 mm^3) within the renal parenchyma was performed on the Dixon fat-only images to avoid contamination with renal sinus or peri-renal fat (**Fig. 1a**). The static magnetic field was homogenized at the voxel location using a first order pencil beam (nine projections) volume static field (B0) shimming algorithm. This method measures nine beams through the voxel of interest and reconstructs the B0 distribution in that voxel. The main advantage of this method is that it is performed in the preparation of the spectroscopy measurement and does not require user input. The location of the shim volumes (50 x 20 x 20 mm^3) was centered around the ^{1}H-MRS voxel. Single voxel Point Resolved Spectroscopy (PRESS) spectra were acquired with an echo time of 40ms, repetition time of 3s for the water-suppressed acquisition (64 signal averages) and 8s for the unsuppressed acquisition (8 averages), ensuring full relaxation of the water and lipid signals (14,15). Spectral bandwidth was 1700 Hz, and 1024 samples were acquired resulting in a spectral resolution of 1.66 Hz/sample. The water-suppressed spectra were acquired using a Multiply Optimized Insensitive Suppression Train (MOIST) suppression method with a bandwidth of 150 Hz. Previous research in cardiac ^{1}H-MRS showed that MOIST performed best at suppression of the water signal, and excitation pulse water suppression should be avoided since this introduces bias in the baseline of the spectra (16). Local power optimization was performed by monitoring the intensity of the water peak and incrementing the tip angles of the excitation pulse and the two refocusing pulses in the PRESS sequence in steps of 5% (range, 90%–150% of the global power optimization result), and selecting the power setting that produced the highest signal intensity. The spectroscopy acquisition was triggered using a pencil beam respiratory navigator technique (17). The navigator volume was placed at the right diaphragm liver-lung interface (**Fig. 1b**), and the spectroscopy measurement was triggered when the diaphragm was in the automatically defined acceptance window of 5mm diaphragm displacement in end-expiration. To further minimize the respiratory motion effects, residual motion was compensated with motion tracking (**Fig. 1c**). To improve navigator stability and performance, the size of the navigator preparation voxel was increased to the same size of the regular navigator voxel. Furthermore, the navigator

signal was improved by using the surface coil rather than the build-in body coil for signal reception. Use of the surface coil resulted in better approximation of the navigator voxel location due to its direct position on top of the body, thereby increasing the respiratory navigator signal.

Intra-examination differences were obtained by repeating the ^{1}H-MRS measurement directly after the first ^{1}H-MRS without repositioning of the subject or changing the position of the surface coil or measurement volumes. Inter-examination variability was studied by repeating the scan protocol after removal and replacement of the subject in the magnet, and subsequent repositioning of the surface coil and measurement volumes. Inter-examination scans were added later in the protocol because of limited research scan time and were therefore not assessed in all participants.

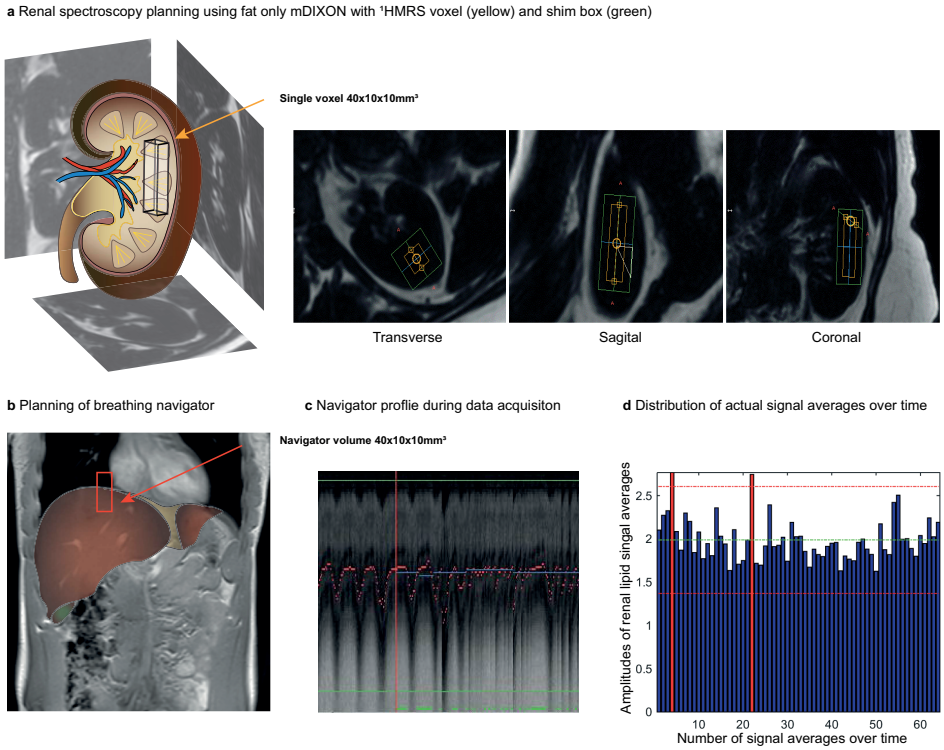

Figure 1. Planning and post-processing analysis of renal ^{1}H-MRS. (a) Planning of single voxel ^{1}H-MRS (yellow) and shim box (green) in renal parenchyma on orthogonal transverse, coronal and sagittal Dixon fat only sequences, (b) planning of breathing navigator at liver-lung interface (c) Navigator profile during acquisition, with bottom white signal form the liver, and dark signal from the lungs. (d) Distribution of amplitudes of renal lipid resonances over time for all water suppressed signal averages. Dotted lines indicate mean amplitude (green) and ± 2.5 SDs (red). Signal averages outside this range were considered outliers and were excluded (marked in red).

Spectral quantification

Acquired spectral raw data output files were reconstructed using an in-house created MATLAB version 8.4 (MathWorks, Natick, Massachusetts, USA) reconstruction script. The raw data was phase corrected after which a weighted sum of the channel signals was calculated for every average. By calculating the phase variation over time, of the unsuppressed spectra, both the unsuppressed and the suppressed spectra were eddy current corrected. Variation in lipid signal amplitude between the signal averages is visualized in **Figure 1d**. Averages outside the 95% confidence interval (CI) were considered outliers and were excluded if present. In the final reconstruction step the included averages were summed. Reconstructed data were fitted in the time domain using Java-based MR User Interface software (jMRUI version 5.0; Katholieke Universiteit Leuven, Leuven, Belgium) (18,19). Residual water signal was removed using the Hankel-Lanczos filter (singular-value decomposition method) (**Fig. 2a**). The Advanced Method for Accurate, Robust and Efficient Spectral fitting (AMARES) algorithm was used to fit the spectra (20). The water suppressed spectra were analyzed using starting values based on known frequency (ppm) and line width (Hz) estimates for renal lipids: triglyceride methyl (CH_3) 0.9 ppm, 10.0 Hz; triglyceride methylene (CH_2)n 1.3 ppm, 13.6 Hz; COO-CH_2 2.1 ppm, 10.0 Hz; trimethylamines (TMA) 3.25 ppm, 8.0 Hz (**Fig. 2b**). As prior knowledge the relative TG resonance frequencies and resonance amplitudes were kept unconstrained, while soft constrains were applied on the linewidth of the resonances: CH_3 0–30 Hz; (CH_2)n 0–30 Hz; COO-CH_2

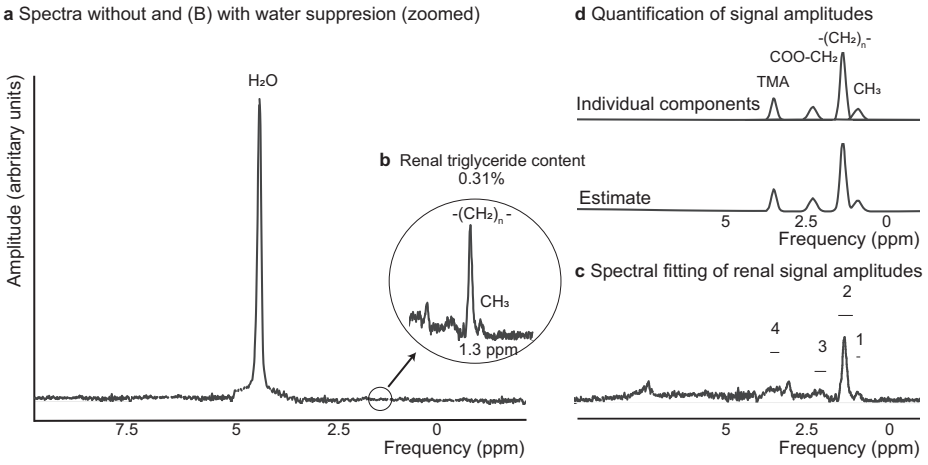

Figure 2. Spectral post-processing of renal ^{1}H-MRS. (a) Single voxel renal ^{1}H-MRS spectra without and with (b) water suppression, resonances from protons of water (peak at 4.7 ppm, H2O), methylene (peak at 1.3 ppm, [CH2]n) and methyl (peak at 0.9 ppm, CH3) are highlighted, (c) Spectral fitting of renal signal amplitudes using estimates for resonances from protons of renal lipids (prior knowledge). Peak number, peak name, frequency, line width: 1. CH3, 0.9 ppm, 10.0 Hz, 2. (CH2)n 1.3 ppm, 13.6 Hz; 3. COO-CH2, 2.1 ppm, 10.0 Hz, 4. TMA 3.25 ppm, 8.0 Hz, (d) AMARES result of individual components of renal lipid signal amplitudes based on original signal and estimated signal using prior knowledge.

0–30 Hz; TMA 0–21 Hz. (**Fig. 2c**). The unsuppressed spectra were analyzed using a starting value of 4.7 ppm for the water signal. All resonances in the suppressed and the unsuppressed spectra were fitted to a Gaussian line shape. Renal TG content was calculated as a percentage of the (unsuppressed) water peak using the following equation:

$$Renal\ TG\% = \frac{triglyceride\ methyl\ (CH_3) + triglyceride\ methylene\ (CH_2)n}{water + triglyceride\ methyl\ (CH_3) + triglyceride\ methylene\ (CH_2)n} \times 100\%$$

Statistical analysis

Renal TG percentages are presented as median (25^{th}, 75^{th} percentile), and other descriptors such as mean (standard deviation SD, range) are also presented. TG percentages were tested for normality using the Shapiro-Wilk test. Logarithmic (log) base 2 transformation of original TG data was performed since renal TG content is not normally distributed (21). Pearson correlations were calculated for first and second measurement of renal log TG% for both intra- and inter-examination measurements. Bland-Altman plots were visualized through a scatterplot of the differences, with reference lines at the mean difference, and mean difference ±2 × SD of the differences (limits of agreement) (22, 23). Back transformed limits of agreement were calculated for intra- and inter-examination measurements by applying $\pm 2\ \overline{X} \times (2^a - 1)/(2^a + 1)$, where $a = \overline{d} \pm 2 \times SD$, $\overline{X}$ is mean TG, and $\overline{d}$ is the mean difference. Group differences in renal TG content between healthy volunteers and T2DM patients were assessed using the Mann-Whitney U test. Two-tailed significance levels of $P<0.05$ were considered to indicate a statistically significant difference. Statistical analyses were performed using STATA version 12.0 (Statacorp, College Station, Texas, USA).

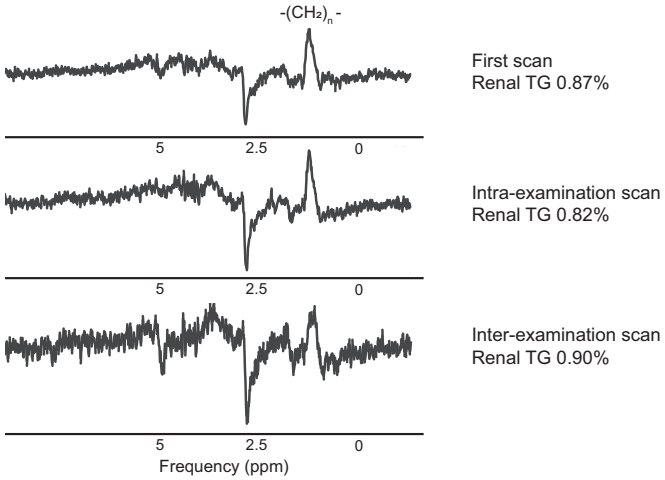

Figure 3. Example of renal ^{1}H-MRS spectra of a healthy volunteer from the three reproducibility acquisitions with corresponding renal TG values.

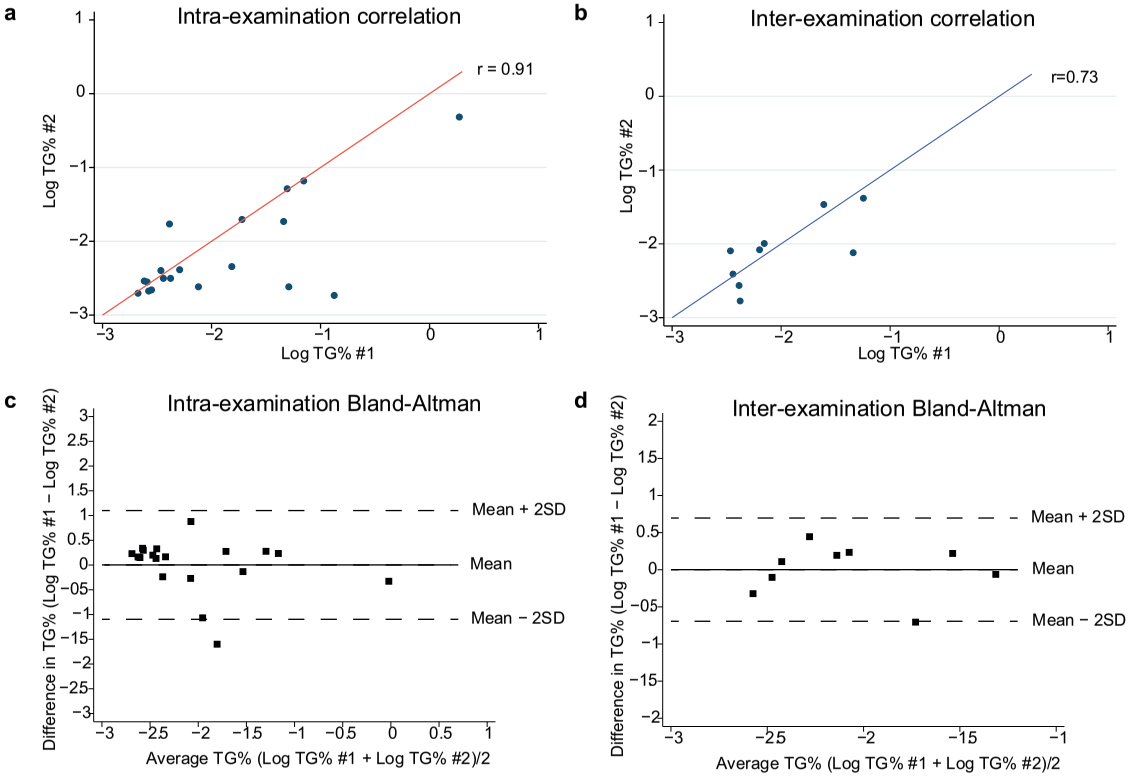

Figure 4. Scatterplots of log-transformed TG with linear fit and Bland-Altman analyses of intra- and inter-examination measurements. (**a**) Scatterplots of within-subject intra-examinations (n=19) with Pearson correlation of 0.91, (**b**) Scatterplots of within-subject inter-examinations (n=9) with Pearson correlation of 0.73. (**c**) Bland-Altman plot of the intra-examination differences (n=19) between measurement #1 and #2 versus the mean of measurement #1 and #2 (mean difference -0.26, lower limit -1.36, upper limit 0.84), (**d**) Bland-Altman plot of the inter-examination differences (n=9) between measurement #1 and #2 versus the mean of measurement #1 and #2 (mean difference -0.07, lower limit -0.77, upper limit 0.62).

RESULTS

Healthy volunteers

Twenty-three healthy participants (mean age 30.1 ± 13.4 years, mean BMI 22.8 ± 5.2 kg/m², 43% men) underwent ^{1}H-MRS for reproducibility assessment (intra-examination n=19, inter-examination n=9). Overall median renal triglyceride content was 0.12% [0.08, 0.22] (range 0.07-1.02%). Both intra-examination (r=0.91) and inter-examination (r=0.73) measurements were highly correlated with first renal TG measurements after log transformation to correct for normality (**Fig. 4 a, b**). Bland-Altman analysis for the intra-examination measurements showed a mean difference of -0.26 log TG% with a lower limit of -1.36 log TG% (95% CI -1.81, -0.90), and a upper limit of agreement of 0.84 log TG% (95% CI 0.38, 1.30) (**Fig. 4c**). For inter-examination measurements, the Bland-Altman analysis showed a mean difference of -0.07 log TG% with a lower limit of -0.77 log TG% (95% CI -1.23, -0.31) and a upper limit of agreement of 0.62 log TG% (95% CI 0.16, 1.08) (**Fig. 4 d**). Corresponding back transformed limits of agreement for intra-examination measurements were -0.89 (95% CI -1.82, -0.90) and 0.57 (95% CI 0.38, 1.30) multiplied by mean TG. For inter-examination measurements back transformed limits of agreement were -0.55 (95% CI -1.31, -0.32) and 0.43 (95% CI 0.13 to 1.11) multiplied by mean TG.

Type 2 diabetes mellitus patients

Fifteen T2DM patients (mean age 59.3 ± 7.0 years, mean BMI 32.9 ± 2.9 kg/m², 47% male) underwent ^{1}H-MRS. Included T2DM patients had a mean creatinine of 73.5 ± 16 umol/L, and mean HbA1c levels of 6.5 ± 1.0%. Median renal TG content in T2DM patients was 0.20% [0.13, 0.22] (range 0.09-0.45). Median renal triglyceride content in T2DM patients was higher compared to healthy volunteers, but observed differences did not reach statistical significance in this small sample size (P=0.08) (**Fig. 5**).

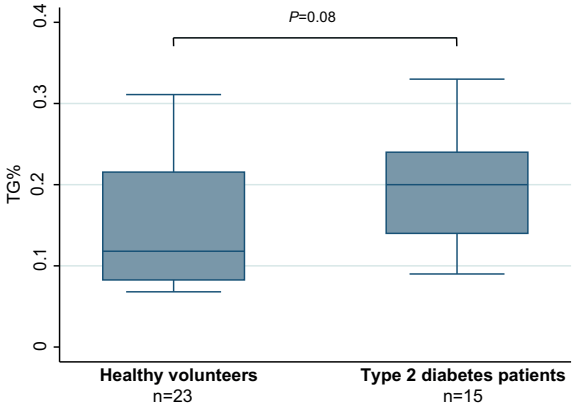

Figure 5. Distribution of renal triglycerides in healthy volunteers and type 2 diabetes patients. Boxplot of renal TG content in 23 healthy volunteers with median TG of 0.12% [0.08, 0.22] (left) and in 15 type 2 diabetes patients with a median TG of 0.20% [0.13, 0.22] (right).

DISCUSSION

We demonstrated that renal metabolic imaging using 3T proton spectroscopy is a reproducible technique that could be used for evaluating the biomarker potential of renal triglyceride in obesity-related renal disease.

We found an overall median renal triglyceride content of 0.12% [0.08, 0.22] in healthy volunteers and 0.20% [0.14, 0.24] in patients with type 2 diabetes. Previously described mean renal triglyceride or fat percentages based on non-invasive human imaging studies range from 0.43 ± 0.10% to 2.18 ± 2.52% (12, 24), however these results are difficult to compare considering technical differences (field strength, acquisition method), and differences in study populations (healthy volunteers, obese participants and type 2 diabetes patients). It has been estimated that the normal human kidney consists of 79.5% water, and overall lipid content in cortex and medulla has been estimated to comprise 0.6% and 1.64% of mean wet kidney weight (25). Obtained renal spectra showed a large peak visible between 1.2 to 1.4 ppm, which predominantly originates from proton resonances of methylene (CH_2) groups of TG. Cholesterol contains methylene groups as well, but these are not visible with current resolution of clinical ^{1}H-MRS since cholesterol is more restricted in its movement (i.e. less magnetic susceptibility or anisotropy due to a greater association with its membranes) resulting in spectral broadening and resonance loss in the background. Based on pathology studies, the estimated overall lipid content in the normal human kidney is composed of approximately one-fifth triglycerides, one-tenth of free fatty acids (non-esterified fatty acids), and the intracellular cholesterol concentration is estimated at one-twentieth or less (25, 26).

Higher levels of renal TG content were observed in type 2 diabetes patients compared to healthy volunteers, but did not reach statistical significance likely due to small sample size. These results need to be validated in a larger cohort with age- and sex-matched controls to draw inferences on whether renal steatosis is truly associated with type 2 diabetes. The underlying mechanisms of fatty kidney have only been investigated in animal models and clinical translation has been hampered by lack of noninvasive tests. A recent pathology study based on nephrectomy specimens found that renal TG content was positively associated with BMI and mainly involved proximal tubule cells, suggesting that renal steatosis is a possible marker of renal fatty acid oversupply (27). These findings have been supported by preclinical studies that showed an increased tubular uptake of free fatty acids (FFAs) in the presence of high FFA plasma concentrations and glomerular albuminuria, which can lead to renal TG storage (6, 28). Low TG storage will most likely not interfere with organ function (e.g. heart, muscle), however excessive renal TG accumulation may lead to tubulointerstitial injury (29, 30) and has been associated with overt albuminuria in obese patients (4). Another potential pathway of renal lipid accumulation and inflammation is increased glucose absorption in hyperglycemia via the

sodium/glucose cotransporter 2 (SGLT2) transporter in proximal tubule cells (31, 32). Improved understanding of renal lipid metabolism in vivo could lead to the identification of potential therapeutic targets for the prevention of obesity-related renal disease, and renal diabetic nephropathy (e.g. fibrates or SGLT-inhibitors) (31). Although the present study shows that ^{1}H-MRS is a reproducible technique for the assessment of renal TG content, several technical limitations exist. The intrinsically low renal TG concentration and voxel size remain important limiting factors of the signal-to-noise ratio even though the field strength in the present study was improved to 3T compared to previous studies at 1.5T. Unintentional locational variation of acquired spectra may be introduced by technical differences in voxel planning and subject repositioning during the examination, which could introduce spectral contamination of non-renal parenchyma tissue such as renal sinus fat and peri-renal fat. Other general technical factors that may affect spectral quality are suboptimal static field shimming, incomplete water suppression, phasing errors, and chemical shift displacement. Since renal ^{1}H-MRS involves metabolites with extremely low concentrations, adequate water suppression and shimming are especially of great importance for sufficient spectral quality. These above-mentioned factors contribute to the inter-subject, intra-examination and inter-examination variability of measured renal TG% by ^{1}H-MRS. Our inter-subject difference (inter-quartile range, IQR) in renal TG% was 0.14% in healthy volunteers, which indicates that the scatter among healthy subjects in their renal fat and renal TG percentages limits the statistical sensitivity to detect significant differences when a single patient or a small group of patients is compared to healthy controls. Inter-subject differences (SDs or IQRs) may reflect technical factors (spectral noise, partial volume effects), and biological variability (low intrinsic renal TG percentages, renal size and cortical thickness).

Intra-examination differences, representing the unchanged position of the ^{1}H-MRS volume and the receive coils, mainly reflect physiologic motion rather than signal-to-noise related variance. One outlier was present in the intra-examination Bland-Altman plot, and was likely due to subject motion in the left-right position that cannot be controlled for by the respiratory navigator. Practical aspects of ^{1}H-MRS measurements, such as the positioning of the surface coil and planning of sensitive volumes are reflected in inter-examination differences. Although calibrations, data acquisition parameters and data post-processing were identical for both measurements, some differences between inter-examination renal TG percentages were present, reflecting measurement variation.

There are several limitations that need to be considered regarding the design of the study. The small sample size of the clinical cohort limits the evaluation of associations between clinical parameters (e.g. BMI, renal function, albuminuria etc.) and renal TG content, as these require adequate adjustment for age, sex, and other possible confounders. Prospective studies are needed to assess to what extent renal TG is associated with renal parameters (glomerular filtration rate, albuminuria, etc.), and to assess potential effects

of medical interventions (glucoregulation, fibrates, statins, stringent weight reduction) on renal triglyceride accumulation (33). Furthermore, we cannot exclude residual effects of fasting on current renal TG measurements (participants were scanned after overnight or ≥4 hours fasting), as this has been described to influence renal TG accumulation in mice (6). Other limitations are the possible influence of intra- and inter-observer variation in the spectral quantification process.

In conclusion, renal metabolic imaging using 3T ^{1}H-MRS is a promising reproducible technique for the assessment of renal triglyceride content that could improve our understanding of obesity-associated renal disease. Further research is needed to assess the potential of renal triglyceride content as a biomarker for obesity-related renal disease.

REFERENCES

1. Ruan XZ, Varghese Z, Moorhead JF. An update on the lipid nephrotoxicity hypothesis. Nat Rev Nephrol. 2009;5(12):713-21.
2. de Vries AP, Ruggenenti P, Ruan XZ, et al. Fatty kidney: emerging role of ectopic lipid in obesity-related renal disease. Lancet Diabetes Endocrinol. 2014;2(5):417-26.
3. D'Agati VD, Chagnac A, de Vries AP, et al. Obesity-related glomerulopathy: clinical and pathologic characteristics and pathogenesis. Nat Rev Nephrol. 2016;12(8):453-71.
4. Li Z, Woollard JR, Wang S, et al. Increased glomerular filtration rate in early metabolic syndrome is associated with renal adiposity and microvascular proliferation. Am J Physiol Renal Physiol. 2011;301(5):F1078-87.
5. Rutledge JC, Ng KF, Aung HH, Wilson DW. Role of triglyceride-rich lipoproteins in diabetic nephropathy. Nat Rev Nephrol. 2010;6(6):361-70.
6. Scerbo D, Son N-H, Sirwi A, et al. Kidney triglyceride accumulation in the fasted mouse is dependent upon serum free fatty acids. J Lipid Res. 2017;58(6):1132-42.
7. Zhou Y, Lin S, Zhang L, Li Y. Resveratrol prevents renal lipotoxicity in high-fat diet-treated mouse model through regulating PPAR-α pathway. Mol Cell Biochem. 2016;411(1-2):143-50.
8. Li L, Zhao Z, Xia J, et al. A long-term high-fat/high-sucrose diet promotes kidney lipid deposition and causes apoptosis and glomerular hypertrophy in bama minipigs. PloS One. 2015;10(11):e0142884.
9. Thomas EL, Hamilton G, Patel N, et al. Hepatic triglyceride content and its relation to body adiposity: a magnetic resonance imaging and proton magnetic resonance spectroscopy study. Gut. 2005;54(1):122-7.
10. Boesch C, Machann J, Vermathen P, Schick F. Role of proton MR for the study of muscle lipid metabolism. NMR Biomed. 2006;19(7):968-88.
11. Rijzewijk LJ, van der Meer RW, Smit JW, et al. Myocardial steatosis is an independent predictor of diastolic dysfunction in type 2 diabetes mellitus. J American Coll Cardiol. 2008;52(22):1793-9.
12. Hammer S, de Vries AP, de Heer P, et al. Metabolic imaging of human kidney triglyceride content: reproducibility of proton magnetic resonance spectroscopy. PLoS One. 2013;8(4):e62209.
13. Jonker JT, de Heer P, Engelse MA, et al. Metabolic imaging of fatty kidney in diabesity: validation and dietary intervention. Nephrol Dial Transplant. 2018 Feb 1;33(2):224-230.